MULTIDIMENSIONAL UPWIND SCHEMES: APPLICATION TO HYDRAULICS

Pilar GARCIA-NAVARRO

Fluid Mechanics. CPS. University of Zaragoza. 50015 Zaragoza. Spain.
e-mail: pigar@posta.unizar.es

Matthew HUBBARD

DAMTP, Silver Street, Cambridge, CB3 9EW, U.K.
e-mail: M.E.Hubbard@damtp.cam.ac.uk

Pilar BRUFAU

Fluid Mechanics. CPS. University of Zaragoza. 50015 Zaragoza. Spain.
e-mail: cuca@ideafix.cps.unizar.es

1 Introduction

Upwind methods are very popular in the modelling of advection dominated flows, and in particular those which contain strong discontinuities. The essence of the upwind method in 1D depends on the reduction of the problem to a set of subproblems that are (almost) independent. The best solution techniques for these scalar subproblems can then be studied carefully and in detail[11]. These methods are frequently used to solve systems of equations in higher dimensions.

One of the recent topics of CFD is accuracy enhancement in multidimensional flow simulations. High resolution upwind schemes for 1D hyperbolic systems of partial differential equations have reduced numerical errors and are successfully used to sharply capture discontinuities. However, extensions of these methods to multidimensional problems do not enhance resolution as much as expected compared with the 1D case[23].

Initial attempts to extend 1D upwind techniques to higher dimensions were all based on 1D upwind concepts applied within a dimensional splitting framework, and modelling the flow by solving simple Riemann problems across cell interfaces. This introduced an undesirable reliance on the computational mesh, and such techniques were not capable of adequately resolving shocks or shears which were not aligned with the grid[4].

Unstructured grids have many advantages for multidimensional flow analysis, particularly their flexibility when constructing boundary fitted grids for complex geometries and their general lack of preferential grid directions. Even so, locally,

schemes based on structured and unstructured grids are the same when the numerical flux normal to the cell face is only evaluated in the 1D manner. The result is a solution algorithm which depends on geometrical variables which have little or no relation to the relevant flow directions. Specifically, cell boundaries are used to define a 1D direction along which the upwinding takes place. Consequently, the choice of the grid has a disproportionate influence on the solution.

It was soon realised that it was necessary to incorporate genuinely multidimensional physics into these algorithms. The first step was taken by Davis[1] who suggested that the shock capturing capabilities of upwind methods could be improved by rotating the Riemann problem to align it with the direction of physically important flow gradients. They take into account variables like flow direction or velocity gradient direction over a cell face as part of the discretization. This work was extended by Levy et al.[12] and Tamura and Fujii[22], but these methods commonly suffered problems with robustness.

An alternative method was developed independently by Rumsey et al.[20] and Parpia and Michalek[16]. Common to these methods is the fact that the multidimensional physics is added at the cell interfaces, thus retaining some 1D aspects. Therefore new multidimensional upwind schemes for equations in more than one space dimension are still being sought which don't assume any one-dimensionality along the grid lines or normal to the cell faces.

The methods discussed in this paper use a genuinely multidimensional physical model for the upwinding which does not fit in to the standard finite volume approach where the representation of the unknowns is considered to be only piecewise continuous. In this respect the new schemes are much closer to finite element methods based on linear elements, with which they share a continuous piecewise linear representation over the cells. On the other hand, they share with upwind methods the properties of asymmetric upwinded stencils and control of monotonicity across discontinuities, and they can be considered as truly multidimensional generalizations of the 1D TVD upwind methods.

The basis of one of the original groups of these multidimensional upwinding techniques is the assumption that any observed gradients in the initial data at the start of a time step are linked to the presence of simple waves in the flow. Since an infinite number of simple wave patterns could be responsible for the same observed gradients, it is necessary to hypothesize the number and nature of the waves present: this is known as a wave model. It is important that the orientation of the waves are not constrained by the directions of the grid. The next idea is to update the solution in a way that acknowledges the direction of propagation of each wave in the model.

The steps to follow for constructing a multidimensional upwind scheme of this type for a non-linear system are the following:

- Construct a suitable scheme for the solution of the scalar advection equation. This involves the development of "fluctuation/residual distribution" techniques in several dimensions. They use a continuous piecewise linear data representation and involve the calculation of the fluctuation (or residual) within each cell and its distribution in an upwind manner to update the flow variables at the vertices.

- Identify the relevant propagation properties and directions within each cell. This requires the development of a wave decomposition model which splits the fluctuations into components, each of which corresponds to a simple wave solution of the equations. The fluctuations due to each scalar wave can then be distributed using an advection scheme from the first step above. Roe developed a number of wave models based on simple waves[17, 18] and Rudgyard, amongst others, independently constructed his own simple wave models[19].

Initial calculations with the simple wave models confirmed an excellent capability to capture oblique discontinuities, for which the multidimensional upwind method was designed, but proved somewhat disappointing in the calculation of smooth (subcritical) flows. This is because the wave models still employ unnecessary dissipation[6].

Deconinck, Hirsch and Peuteman[2] concurrently devised their own alternative strategy for decomposing the fluctuation. This was based on an attempt to find an approximate diagonalization of the system of equations via an appropriate similarity transformation. The original schemes lacked robustness but the idea has subsequently been improved upon by applying the diagonalization technique to a preconditioned set of equations. The correct choice of preconditioner leads to a maximally decoupled system of equations and provides a very accurate method for calculating steady state solutions to nonlinear systems of conservation laws[7, 14, 15].

Upwind finite volume schemes are improved by higher order interpolation, where more than the direct neighbour points are used. This is not the case for multidimensional upwind schemes, but accuracy remains a critical issue. Where steady state solutions are of interest, an essential feature of a numerical scheme is the convergence towards those steady states. Therefore, care has to be taken to provide reasonable convergence properties for multidimensional upwind scheme, in order for them to be competitive with other methods, and the issue of convergence acceleration has been studied in some detail[7]. Unsteady problems have only really been studied in depth more recently, and then mainly in the scalar case[10, 8], but evidence will be presented in this paper that even the schemes developed for steady state problems provide a significant improvement in the modelling of nonlinear problems over comparable finite volume schemes. Even so, it has become apparent that a rather fundamental distinction should be made between computational methods for steady and unsteady flows. The simple wave model approach is discussed in some detail here, not because it gives the best steady state solutions, but because it currently appears to be the most appropriate form of multidimensional upwinding for application to time-dependent problems.

The issue of approximating source terms is also discussed briefly, and suggestions made as to how they should be incorporated within the overall discretisation in order to maintain the accuracy of the homogeneous scheme, something which has so far proved to be simpler for the diagonalization approach.

2 Basic Scalar Technique

The technique for 2D problems assumes that the physical domain is discretized using triangular cells (these methods are less naturally applied to quadrilaterals[7]) and a set of solution values is stored at the nodes of the mesh. For each cell T, and for a linear scalar equation of the form

$$\frac{\partial w}{\partial t} + \mathbf{a} \cdot \nabla w = 0, \qquad \mathbf{a} = (a_x, a_y) \tag{1}$$

where $\mathbf{a}$ is a constant vector, the fluctuation is defined as

$$\phi_T = \int_T \frac{\partial w}{\partial t} dS = -\int_T \mathbf{a} \cdot \nabla w dS \tag{2}$$

and the closely related quantity, the cell residual R_T, as

$$R_T = -\frac{1}{S_T}\phi_T = \frac{1}{S_T}\int_T \mathbf{a} \cdot \nabla w dS = -\frac{1}{S_T}\oint_C w\mathbf{a} \cdot \hat{\mathbf{n}} dC \tag{3}$$

where C represents the cell boundary and $\mathbf{n}$ the inward normal to that boundary. Note that the final expression in (3) is only valid if $\nabla \cdot \mathbf{a} = 0$. The fluctuation contains information on the state of the cell and the distribution of this information to the nodes must be done in a way which ensures conservation[5].

From the properties of the normals in the cell and the additional assumption that the solution varies linearly within each element, it is possible to identify a discrete approximation of ∇w[4],

$$\nabla w_T = \frac{1}{2S_T}\sum_{i=1}^{3} w_i \mathbf{n}_i \tag{4}$$

such that

$$R_T = \frac{1}{S_T}\int_T \mathbf{a} \cdot \nabla w dS = \frac{1}{S_T}\mathbf{a} \cdot \nabla w_T \int_T dS = \mathbf{a} \cdot \nabla w_T. \tag{5}$$

Equivalently,

$$\phi_T = -\sum_{i=1}^{3} w_i k_i \tag{6}$$

which introduces the quantities $k_i = \frac{1}{2}\mathbf{a} \cdot \mathbf{n}_i$, containing information about the direction of the advection speed relative to the cell edges. The k_i can be used to decide whether flow enters or leaves the triangle through a particular edge and, in that sense, form a useful tool for imposing the upwind properties of the method.

Residuals and fluctuations are both cell-based quantities, and will be used to update the nodal solution values. For this purpose we need to introduce quantities known as distribution coefficients, D_T^i. By using a simple forward Euler time

differencing the following procedure can now be defined to update the variables at all the nodes in a single cell

$$\begin{aligned} S_1 w_1^{n+1} &= S_1 w_1^n - \Delta t S_T D_T^1 R_T^n \\ S_2 w_2^{n+1} &= S_2 w_2^n - \Delta t S_T D_T^2 R_T^n \\ S_3 w_3^{n+1} &= S_3 w_3^n - \Delta t S_T D_T^3 R_T^n \end{aligned} \tag{7}$$

where $S_i = \frac{1}{3}\sum_{T_i} S_T$ is the area of the median dual cell around node i, one third the total area of the triangles having i as vertex. Note that for simplicity a cell residual only contributes to its own vertices, so the condition $\sum_{i=1}^{3} D_T^i = 1$ ensures conservation and consistency.

There exist many criteria for the design of advection schemes according to the choice of the distribution coefficients D_T^i. Two properties are of prime interest, positivity and linearity preservation:

- Positivity means that every solution value at the new time level can be written as a convex combination of old solution values, and is related to the 1D property of monotonicity.
- Linearity preservation has to do with higher order accuracy. It requires that the scheme preserves the exact steady state solution whenever this is a linear function in space, and for an arbitrary triangulation of the domain. This is closely related to the idea of second order accuracy in the context of finite difference schemes, although it is an accuracy requirement on the steady state space discretization only. Less accuracy is gained in the time-dependent case, but it is still significant.

It can be proved that a linear scheme cannot be both positive and linearity preserving[5], a result which is closely related to Godunov's theorem on the incompatibility between second order accuracy and monotonicity preservation for linear schemes in one dimension. Therefore, in order to have both of the above properties, nonlinear schemes must be considered where the update coefficients depend on the data. This leads to the generation of nonlinear schemes even for linear equations. The most commonly used of these nonlinear schemes is the PSI scheme[7] which is based on the linear, positive N scheme, and can be thought of in one of two ways. In its original derivation, it is based on the combination of optimal positive upwind (N) schemes based on two distinct advection velocities, the usual one $\mathbf{a}$, and its component in the direction of the local solution gradient, $(\mathbf{a}\cdot\hat{\nabla}w)\hat{\nabla}w$. More recently, it was written as the N scheme combined with a form of cross-stream limiter[21].

The underlying advection schemes used for the shallow water equations are no different to those used for the Euler equations so we will not go into further detail about their particular construction and description. We refer the reader to the very good reviews in [7] and [5].

2.1 Nonlinear equations

It should be noted that when the equation itself is nonlinear a suitable linearization must be performed before the technique described above for a linear equation

is applied. In simple cases an averaged advection speed which satisfies discrete conservation can be found by assuming linear variation of the conserved quantities w over the cell, leading to a constant gradient ∇w. However, a general nonlinear 2D system of conservation laws of the form

$$\frac{\partial \mathbf{U}}{\partial t} + \nabla \cdot \mathbf{F} = 0, \qquad \mathbf{F} = (\mathbf{f}, \mathbf{g}) \tag{8}$$

requires the construction of an appropriate discrete form of the system

$$\frac{\partial \mathbf{U}}{\partial t} + (\mathbf{A}, \mathbf{B}) \cdot \nabla \mathbf{U} = 0. \tag{9}$$

In particular, a consistent approximation for the cell residual is sought

$$\mathbf{R}_T = \frac{1}{S_T} \int_T (\mathbf{A}, \mathbf{B}) \cdot \nabla \mathbf{U} dS = (\tilde{\mathbf{A}}_T, \tilde{\mathbf{B}}_T) \cdot \nabla \mathbf{U}_T \tag{10}$$

where $\tilde{\mathbf{A}}_T$, $\tilde{\mathbf{B}}_T$ are discrete averages of the Jacobian matrices, constructed from the nodal values. Now, assuming linear variation of the conservative variables $\mathbf{U}$ over each cell enables us to write

$$\mathbf{R}_T = \frac{1}{S_T} \nabla \mathbf{U}_T \cdot \int_T (\mathbf{A}, \mathbf{B})\, dS \tag{11}$$

from which discrete cell gradients and cell Jacobians can be defined:

$$\tilde{\mathbf{A}} = \frac{1}{S_T} \int_T \mathbf{A} dS\ , \qquad \tilde{\mathbf{B}} = \frac{1}{S_T} \int_T \mathbf{B} dS. \tag{12}$$

Unfortunately, the exact evaluation of the above integrals is not practical either for the Euler or for the shallow water equations. Roe et al.[3] suggested the introduction of "parameter vector" variables for a simpler treatment of the former system. The strategy followed for the shallow water equations is similar and makes use of the set of primitive variables, but there is no set of variables which can quite play the role of the parameter vector, as will be discussed in the following section.

3 The 2D Shallow Water System

In the conservative and homogeneous version of the shallow water system of equations with independent variables $\mathbf{U} = (h, hu, hv)^T$, where h, u and v are the depth and x- and y-velocities respectively, the fluxes are

$$\mathbf{f} = \left(hu, hu^2 + g\frac{h^2}{2}, huv \right)^T, \qquad \mathbf{g} = \left(hv, huv, hv^2 + g\frac{h^2}{2} \right)^T. \tag{13}$$

and the residual is defined as (*cf.* Equation (10))

$$\mathbf{R}_T = \frac{1}{S_T} \int_T (\mathbf{f}_x + \mathbf{g}_y)\, dS = -\frac{1}{S_T} \oint_C (\mathbf{f}, \mathbf{g}) \cdot \hat{\mathbf{n}}\ dC. \tag{14}$$

We are seeking a conservative linearization of the Jacobians satisfying

$$\mathbf{R}_T = \tilde{\mathbf{f}}_x + \tilde{\mathbf{g}}_y = \tilde{\mathbf{A}}\tilde{\mathbf{U}}_x + \tilde{\mathbf{B}}\tilde{\mathbf{U}}_y. \tag{15}$$

In order to simplify the subsequent evaluation of the discrete flux Jacobians (*cf.* Equation (12)) we can use the transformation matrix $\mathbf{M} = \frac{\partial \mathbf{U}}{\partial \mathbf{V}}$ to move from the conserved variables $\mathbf{U}$ to the primitive variables $\mathbf{V} = (h, u, v)^T$. This requires the definition of new Jacobian matrices, $\mathbf{S}$ and $\mathbf{T}$, as

$$\mathbf{S} = \frac{\partial \mathbf{f}}{\partial \mathbf{V}} = \frac{\partial \mathbf{f}}{\partial \mathbf{U}}\frac{\partial \mathbf{U}}{\partial \mathbf{V}} = \mathbf{A}\mathbf{M} \ , \qquad \mathbf{T} = \frac{\partial \mathbf{g}}{\partial \mathbf{V}} = \frac{\partial \mathbf{g}}{\partial \mathbf{U}}\frac{\partial \mathbf{U}}{\partial \mathbf{V}} = \mathbf{B}\mathbf{M} \tag{16}$$

so that

$$\mathbf{f}_x + \mathbf{g}_y = \mathbf{f}_\mathbf{V}\mathbf{V}_x + \mathbf{g}_\mathbf{V}\mathbf{V}_y = \mathbf{S}\mathbf{V}_x + \mathbf{T}\mathbf{V}_y. \tag{17}$$

Under the assumption that the variables $\mathbf{V}$ are linear over the cells T the gradients $\nabla\mathbf{V}$ are constant, and this enables us to write the residual as

$$\begin{aligned} \mathbf{R}_T &= \frac{1}{S_T}\int_T \left(\mathbf{S}\left(\mathbf{V}\right)\mathbf{V}_x + \mathbf{T}\left(\mathbf{V}\right)\mathbf{V}_y\right) dS \\ &= \frac{1}{S_T}\left(\int_T \mathbf{S}\left(\mathbf{V}\right) dS\right)\mathbf{V}_x + \left(\int_T \mathbf{T}\left(\mathbf{V}\right) dS\right)\mathbf{V}_y = \tilde{\mathbf{S}}\mathbf{V}_x + \tilde{\mathbf{T}}\mathbf{V}_y \end{aligned} \tag{18}$$

with the definitions

$$\tilde{\mathbf{S}} = \frac{1}{S_T}\int_T \mathbf{S}\left(\mathbf{V}\right) dS \ , \qquad \tilde{\mathbf{T}} = \frac{1}{S_T}\int_T \mathbf{T}\left(\mathbf{V}\right) dS. \tag{19}$$

We can evaluate $\tilde{\mathbf{S}}$ and $\tilde{\mathbf{T}}$ exactly, since $\mathbf{S}$ and $\mathbf{T}$ both vary quadratically with $\mathbf{V}$ but, in order for the wave model to be employed, the approximate Jacobians are required to take the form $\tilde{\mathbf{S}} = \mathbf{S}(\tilde{\mathbf{V}})$ and $\tilde{\mathbf{T}} = \mathbf{T}(\tilde{\mathbf{V}})$. $\tilde{\mathbf{V}}$ can be simply calculated by averaging over the nodal values at the vertices of the triangle T but, unlike with the Euler equations, this leaves a small correction term which must be added for conservation[9] (and depends on the choice of independent variables $\mathbf{V}$).

We can now reverse the transformation to define linearized derivatives of the conservative variables,

$$\tilde{\mathbf{U}}_x = \mathbf{M}(\tilde{\mathbf{V}})\nabla\mathbf{V}_x \ , \qquad \tilde{\mathbf{U}}_y = \mathbf{M}(\tilde{\mathbf{V}})\nabla\mathbf{V}_y \tag{20}$$

and rewrite

$$\mathbf{R}_T = \tilde{\mathbf{R}}\mathbf{M}^{-1}(\tilde{\mathbf{V}})\tilde{\mathbf{U}}_x + \tilde{\mathbf{S}}\mathbf{M}^{-1}(\tilde{\mathbf{V}})\tilde{\mathbf{U}}_y = \tilde{\mathbf{A}}\tilde{\mathbf{U}}_x + \tilde{\mathbf{B}}\tilde{\mathbf{U}}_y \tag{21}$$

where $\mathbf{M} = \frac{\partial \mathbf{U}}{\partial \mathbf{V}}$, which allows the identification of $\tilde{\mathbf{A}}$ and $\tilde{\mathbf{B}}$.

Having carried out this linearization, we have to compute the discrete residuals $\mathbf{R}_T$ (or fluctuations $\phi_T = -S_T\mathbf{R}_T$) and distribute them to the vertices of the cells by means of an advection scheme (as discussed in Section 2). For this purpose it is necessary to decompose the residual into simple pieces, for example scalar components that can be explained as due to the passage of a simple wave. This requires a description of the wave models.

4 Simple Wave Models

Consider the linearized system of equations written in primitive variables

$$\frac{\partial \mathbf{V}}{\partial t} + \tilde{\mathbf{E}}\frac{\partial \mathbf{V}}{\partial x} + \tilde{\mathbf{H}}\frac{\partial \mathbf{V}}{\partial y} = 0. \tag{22}$$

A simple wave solution can be found according to Roe[17, 18] in the form

$$\mathbf{V} = \mathbf{V}(\xi) \quad \text{with} \quad \xi = x\mathbf{n}_\theta - \lambda_\theta t \tag{23}$$

where $\mathbf{n}_\theta = (\cos\theta, \sin\theta)$ gives the direction of propagation and λ_θ the speed of the particular wave. It is possible then to express the gradient of the independent variables as a sum

$$\nabla\mathbf{V} = \sum_{k=1}^{N_w} \alpha^k \mathbf{r}^k \mathbf{n}^k \ , \qquad \mathbf{n}^k = (\cos\theta^k, \sin\theta^k) \tag{24}$$

in which N_w is the number of waves in the decomposition. Equivalently,

$$\mathbf{V}_x = \sum_{k=1}^{N_w} \alpha^k \mathbf{r}^k \cos\theta^k \ , \qquad \mathbf{V}_y = \sum_{k=1}^{N_w} \alpha^k \mathbf{r}^k \sin\theta^k. \tag{25}$$

The vectors $\mathbf{r}^k$ are right eigenvectors of the matrix $\mathbf{M}^* = \tilde{\mathbf{E}}\cos\theta + \tilde{\mathbf{H}}\sin\theta$ and take one of three forms (representing two types of gravity wave and a shear wave):

$$\mathbf{r}_{G1} = \begin{pmatrix} 1 \\ \frac{g}{\tilde{c}}\cos\theta \\ \frac{g}{\tilde{c}}\sin\theta \end{pmatrix}, \qquad \mathbf{r}_{G2} = \begin{pmatrix} 1 \\ -\frac{g}{\tilde{c}}\cos\theta \\ -\frac{g}{\tilde{c}}\sin\theta \end{pmatrix}, \qquad \mathbf{r}_S = \begin{pmatrix} 0 \\ -\sin\theta \\ \cos\theta \end{pmatrix}, \tag{26}$$

where $\tilde{c}$ is the velocity of small perturbations in still water, the equivalent of the speed of sound in gas-dynamics, and is given by $\tilde{c} = (g\tilde{h})^{1/2}$. The variables α^k represent weighting coefficients of the sum and θ^k are the propagation angles of each wave.

The connection between the gradient of the primitive variables and that of the averaged conservative variables (20) can be used to develop the latter as

$$\tilde{\mathbf{U}}_x = \sum_{k=1}^{N_w} \alpha^k \mathbf{r}_c^k \cos\theta^k \ , \quad \tilde{\mathbf{U}}_y = \sum_{k=1}^{N_w} \alpha^k \mathbf{r}_c^k \sin\theta^k \tag{27}$$

where now, $\mathbf{r}_c^k$ represent the right eigenvectors of the matrix $\mathbf{M}^* = \tilde{\mathbf{A}}\cos\theta + \tilde{\mathbf{B}}\sin\theta$ and can be calculated using the relationship $\mathbf{r}_c^k = \mathbf{M}(\tilde{\mathbf{V}})\mathbf{r}^k$. It is worth noting here that the two matrices $\mathbf{M}^*$ and $\mathbf{M}_c^*$ share the same set of eigenvalues (or wave speeds) λ^k given, for the three wave types, by

$$\begin{aligned} \lambda_{G1} &= \tilde{u}\cos\theta + \tilde{v}\sin\theta + \tilde{c} \\ \lambda_{G2} &= \tilde{u}\cos\theta + \tilde{v}\sin\theta - \tilde{c} \\ \lambda_S &= \tilde{u}\cos\theta + \tilde{v}\sin\theta. \end{aligned} \tag{28}$$

Note that by implication α, λ and $\mathbf{r}$ are all evaluated at the cell average state $\tilde{\mathbf{V}}$ (see previous section). It now follows from (27) that the residual then can be split into a sum of waves

$$\mathbf{R}_T \;=\; \tilde{\mathbf{A}}\tilde{\mathbf{U}}_x + \tilde{\mathbf{B}}\tilde{\mathbf{U}}_y \;=\; \sum_{k=1}^{N_w} \alpha^k \lambda^k \mathbf{r}_c^k \tag{29}$$

so that it can be written in the form

$$\mathbf{R}_T = \sum_{k=1}^{N_w} \left(\lambda^k \cdot \nabla w^k\right) \mathbf{r}_c^k \tag{30}$$

for appropriate choices of the wave velocities λ^k and "characteristic" gradient ∇w. This is simply a sum of components of precisely the form seen in (5).

We next describe two of the most successful simple wave models proposed in the literature as suitable to accomplish the above decomposition.

4.1 Roe's wave models

The wave decomposition of the gradient of the primitive variables,

$$\nabla \mathbf{V} = \sum_{k=1}^{N_w} \alpha^k \mathbf{r}^k \mathbf{n}^k, \tag{31}$$

represents a system of six equations in the 2D shallow water case, where we have two spatial derivatives for each of the three variables. Therefore, it allows for six unknowns. These must correspond to coefficients or angles of propagation of suitable choices of waves whose advection will represent the total fluctuation.

Following Roe's suggested Model D for the treatment of the Euler equations[17], a splitting can be made into four orthogonal acoustic waves, labelled by their strengths (coefficients) and one angle θ which determines the four directions (α_1, θ), $(\alpha_2, \theta + \pi)$, $\left(\alpha_3, \theta + \frac{\pi}{2}\right)$, $\left(\alpha_4, \theta + \frac{3\pi}{2}\right)$, along with one shear wave (β, ϕ) of strength β at an angle ϕ. The six unknowns are taken to be α_1, α_2, α_3, α_4, β and θ. The value of the angle ϕ is determined in terms of the solution as

$$\phi = \theta - \frac{\pi}{4}\text{sign}\left(\beta\right). \tag{32}$$

Making use of the equivalents of the basic trigonometric functions to those of the first quadrant of the unit radius circle, and after some algebraic manipulations,

$$\beta = v_x - u_y \;, \qquad \tan 2\theta = \frac{u_y + v_x}{u_x - v_y} \tag{33}$$

and

$$\alpha_1 \;=\; \frac{1}{2}\left(h_x \cos\theta + h_y \sin\theta + \frac{c}{g}\left(\frac{u_x \cos^2\theta - v_y \sin^2\theta}{\cos 2\theta} - \frac{1}{2}|\beta|\right)\right) \tag{34}$$

$$
\begin{aligned}
\alpha_2 &= \frac{1}{2}\left(-\left(h_x\cos\theta + h_y\sin\theta\right) + \frac{c}{g}\left(\frac{u_x\cos^2\theta - v_y\sin^2\theta}{\cos 2\theta} - \frac{1}{2}|\beta|\right)\right)\\
\alpha_3 &= \frac{1}{2}\left(h_y\cos\theta - h_x\sin\theta + \frac{c}{g}\left(\frac{v_y\cos^2\theta - u_x\sin^2\theta}{\cos 2\theta} + \frac{1}{2}|\beta|\right)\right)\\
\alpha_4 &= \frac{1}{2}\left(-\left(h_y\cos\theta - h_x\sin\theta\right) + \frac{c}{g}\left(\frac{v_y\cos^2\theta - u_x\sin^2\theta}{\cos 2\theta} + \frac{1}{2}|\beta|\right)\right).
\end{aligned}
$$

λ and ∇w are then constructed so that the advection velocities each take one of the appropriate forms represented by

$$
\lambda_{G1} = \begin{pmatrix} u + c\cos\theta \\ v + c\sin\theta \end{pmatrix}, \quad \lambda_{G2} = \begin{pmatrix} u - c\cos\theta \\ v - c\sin\theta \end{pmatrix}, \quad \lambda_S = \begin{pmatrix} u \\ v \end{pmatrix}. \tag{35}
$$

The main problems with this model are that it has more than three waves and so introduces unnecessary numerical dissipation, and the dependence of the propagation directions on solution gradients hinders convergence to the steady state.

4.2 Rudgyard's wave models

Rudgyard[19] based his wave models on the idea of obtaining the six waves by choosing two, in principle, arbitrary propagation angles, θ_1 and θ_2, and performing a decomposition of the gradient of the form

$$
\nabla\mathbf{V} = \sum_{k=1}^{3}\alpha_{\theta_1}^k\mathbf{r}_{\theta_1}^k\mathbf{n}_{\theta_1} + \sum_{k=1}^{3}\alpha_{\theta_2}^k\mathbf{r}_{\theta_2}^k\mathbf{n}_{\theta_2} \tag{36}
$$

which contains six free parameters, the six coefficients α_θ^k. The vectors $\mathbf{n}_\theta = (\cos\theta, \sin\theta)$ are again unit vectors in the direction θ, and $\mathbf{r}_\theta^k$ are the right eigenvectors of the matrix $\mathbf{M}^*$, as defined in (26) (a full set of eigenvectors is used in the decomposition for each of θ_1 and θ_2). In order to solve for the unknowns, use is also made of the left eigenvectors of that matrix

$$
\mathbf{l}_\theta^{G1} = \begin{pmatrix} \frac{1}{2} \\ \frac{c}{2g}\cos\theta \\ \frac{c}{2g}\sin\theta \end{pmatrix}, \quad \mathbf{l}_\theta^{G2} = \begin{pmatrix} \frac{1}{2} \\ -\frac{c}{2g}\cos\theta \\ -\frac{c}{2g}\sin\theta \end{pmatrix}, \quad \mathbf{l}_\theta^{S} = \begin{pmatrix} 0 \\ -\sin\theta \\ \cos\theta \end{pmatrix} \tag{37}
$$

and of the unit vector normal to $\mathbf{n}_\theta$, $\mathbf{s}_\theta = (-\sin\theta, \cos\theta)$, leading to

$$
\alpha_{\theta_1}^k = -\frac{\mathbf{s}_{\theta_2}\cdot\left(\mathbf{l}_{\theta_1}^k\cdot\nabla\mathbf{V}\right)}{\sin\left(\theta_2 - \theta_1\right)}, \qquad \alpha_{\theta_2}^k = \frac{\mathbf{s}_{\theta_1}\cdot\left(\mathbf{l}_{\theta_2}^k\cdot\nabla\mathbf{V}\right)}{\sin\left(\theta_2 - \theta_1\right)}. \tag{38}
$$

In this case the associated advection velocities in (30) are chosen so that, from (38), $\nabla w^k = \mathbf{l}_\theta^k\cdot\nabla\mathbf{V}$.

The best of the options proposed for Rudgyard's wave models is the choice of angles which satisfy the equation $u\cdot\mathbf{n}_\theta - c = 0$, that is, those angles that make

the velocity of one of the gravity waves vanish. They do not depend on solution gradients and can be expressed as

$$\theta_1 = \arctan\left(\frac{v + u\sqrt{F^2-1}}{u - v\sqrt{F^2-1}}\right) , \qquad \theta_2 = \arctan\left(\frac{v - u\sqrt{F^2-1}}{u + v\sqrt{F^2-1}}\right) , \tag{39}$$

with $F^2 = \frac{u^2+v^2}{c^2}$ representing the Froude number (or the Mach number in the gas dynamics problem). This technique gives very good results for supercritical flows but is not directly applicable to the subcritical case. It can nevertheless be adapted for subcritical flows by replacing $F^2 - 1$ with $\max\left(F^2 - 1, \epsilon\right)$. The tolerance ϵ typically takes a value of 0.01. Results become increasingly poor as the Froude number decreases and the effect of having more than three waves becomes more significant.

5 Approximate Diagonalizations

In 1D shallow water flows it is possible to diagonalize the flux Jacobian, thus splitting the problem into independent scalar subproblems. Unfortunately, in 2D the matrices $\mathbf{A}$ and $\mathbf{B}$ cannot generally be diagonalized simultaneously (hence the difficulty in constructing suitable wave models). Instead, an approximate diagonalization can be constructed via a 3-parameter similarity transformation [2], giving a system in 'characteristic' variables $\mathbf{W}$,

$$\mathbf{W}_t + \mathbf{A}_W \mathbf{W}_x + \mathbf{B}_W \mathbf{W}_y \;=\; \mathbf{0} \, , \tag{40}$$

in which the 3 free parameters are chosen so that the new Jacobians $\mathbf{A}_W$ and $\mathbf{B}_W$ are, in some sense, close to being diagonal. This is treated as a decoupled set of inhomogeneous equations, each with a residual of the form

$$R_T \;=\; \lambda \cdot \nabla w + q \, , \tag{41}$$

(the distribution coefficients can be calculated as they would for the homogeneous fluctuation but then used to distribute the complete R_T) and a conservative flux balance,

$$\mathbf{R}_T \;=\; \sum_{k=1}^{N_{eq}} \left(\lambda^k \cdot \nabla w^k + q^k\right) \mathbf{r}_c^k \, , \tag{42}$$

in which $\mathbf{r}_c^k$ are the columns of the similarity transformation matrix $\frac{\partial \mathbf{U}}{\partial \mathbf{W}}$, and $N_{eq} = 3$ is the number of equations in the system.

These methods have an advantage over the existing simple wave models in having the correct number of components for linearity preservation ($N_w = N_{eq}$) but the propagation directions, which depend on the parameters which define the similarity transformation, are usually chosen to depend on solution gradients, creating problems with convergence to a steady state. However, their main disadvantage is the presence of the source terms q^k which destroy positivity and hence robustness.

The effect of the source terms created by the characteristic decomposition can be minimised by attempting to diagonalize a preconditioned form of the shallow

water equations [15, 14]. The decomposed flux balance once more takes the form (42), but now $\mathbf{r}_c^k$ are the columns of the matrix $\frac{\partial \mathbf{U}}{\partial \mathbf{Q}}\mathbf{P}^{-1}\frac{\partial \mathbf{Q}}{\partial \mathbf{W}}$, $\mathbf{Q}$ being an intermediate set of (symmetrizing) variables, introduced to simplify the algebra, and $\mathbf{P}$ a preconditioning matrix. Careful choice of the preconditioner gives an optimal decoupling of the system, complete in supercritical flow but unavoidably including a coupled 2×2 elliptic subsystem for subcritical flow.

Briefly, these most recent decompositions are constructed by first transforming the shallow water equations into symmetrizing variables,

$$\partial \mathbf{Q} \;=\; \begin{pmatrix} \sqrt{\frac{g}{d}}\,\partial d \\ \partial q \\ q\,\partial\theta \end{pmatrix} , \tag{43}$$

where $q = \sqrt{u^2 + v^2}$ is the flow speed and $\theta = \tan^{-1}\left(\frac{v}{u}\right)$ is the direction of the flow. The system therefore becomes

$$\mathbf{Q}_t + \mathbf{A}_Q \mathbf{Q}_x + \mathbf{B}_Q \mathbf{Q}_y \;=\; \mathbf{0} \,, \tag{44}$$

in which the flux Jacobians are symmetric matrices given by

$$\mathbf{A}_Q \;=\; \frac{\partial \mathbf{Q}}{\partial \mathbf{U}}\mathbf{A}\frac{\partial \mathbf{U}}{\partial \mathbf{Q}} \,, \qquad \mathbf{B}_Q \;=\; \frac{\partial \mathbf{Q}}{\partial \mathbf{U}}\mathbf{B}\frac{\partial \mathbf{U}}{\partial \mathbf{Q}}. \tag{45}$$

The equations (44) are simplified even further when they are written in terms of the streamwise coordinates, ξ and η, which leads to

$$\mathbf{Q}_t + \mathbf{A}_Q^S \mathbf{Q}_\xi + \mathbf{B}_Q^S \mathbf{Q}_\eta \;=\; \mathbf{0} \,, \tag{46}$$

where

$$\mathbf{A}_Q^S \;=\; \frac{u\mathbf{A}_Q + v\mathbf{B}_Q}{q} \,, \qquad \mathbf{B}_Q^S \;=\; \frac{-v\mathbf{A}_Q + u\mathbf{B}_Q}{q} \,. \tag{47}$$

These equations are now preconditioned by an appropriate matrix $\mathbf{P}$, giving

$$\mathbf{Q}_t + \mathbf{P}\left(\mathbf{A}_Q^S \mathbf{Q}_\xi + \mathbf{B}_Q^S \mathbf{Q}_\eta\right) \;=\; \mathbf{0} \,, \tag{48}$$

and this system is transformed into "characteristic" variables,

$$\mathbf{W}_t + \mathbf{A}_W^S \mathbf{W}_\xi + \mathbf{B}_W^S \mathbf{W}_\eta \;=\; \mathbf{0} \,, \tag{49}$$

which can be treated as (40), but where

$$\mathbf{A}_W^S \;=\; \frac{\partial \mathbf{W}}{\partial \mathbf{Q}}\mathbf{P}\mathbf{A}_Q^S\frac{\partial \mathbf{Q}}{\partial \mathbf{W}} \,, \qquad \mathbf{B}_W^S \;=\; \frac{\partial \mathbf{W}}{\partial \mathbf{Q}}\mathbf{P}\mathbf{B}_Q^S\frac{\partial \mathbf{Q}}{\partial \mathbf{W}}. \tag{50}$$

For an appropriate choice of $\mathbf{P}$ the system (49) is either fully or partially diagonalized depending on whether the flow is supercritical or subcritical. The hyperbolic components are treated using the standard scalar schemes, but the subcritical elliptic subsystem can usefully be distributed in a different manner: a system Lax-Wendroff scheme has been shown to work well with this component[14].

An example of a suitable preconditioner, based on that of Mesaros and Roe[14], is given by[9]

$$\mathbf{P} \;=\; \frac{1}{q}\begin{pmatrix} \frac{\varepsilon F^2}{\beta\kappa} & -\frac{\varepsilon F}{\beta\kappa} & 0 \\ -\frac{\varepsilon F}{\beta\kappa} & \frac{\varepsilon}{\beta\kappa}+\varepsilon & 0 \\ 0 & 0 & \frac{\beta}{\kappa} \end{pmatrix}, \tag{51}$$

where

$$\beta \;=\; \sqrt{|F^2-1|}\;, \qquad \kappa \;=\; \max(F,1)\;, \tag{52}$$

and $\varepsilon = \varepsilon(F)$ is a function which satisfies $\varepsilon(0) = \frac{1}{2}$ and $\varepsilon(F) = 1$ for $F \geq 1$ (giving the correct behaviour in the preconditioned system at stagnation and continuity of the optimal decomposition through the critical point).

These preconditioned wave models have proved to be the best of the current decompositions for the modelling of steady state problems but, in contrast to the simple wave models, seem unlikely to provide a simple extension to unsteady problems (not least because they have a singularity at stagnation points which can only be treated in the steady case).

6 Source terms

The modelling of shallow water flows commonly requires the inclusion of source terms, and hence the approximation of inhomogeneous equations of the form

$$\frac{\partial \mathbf{U}}{\partial t} + \nabla \cdot \mathbf{F} = \mathbf{S}. \tag{53}$$

For example, taking

$$\mathbf{S} = (0, -ghz_x, -ghz_y)^T \tag{54}$$

allows the modelling of flow over a varying bed topography, defined by the gradient of the bed height, ∇z.

In principle it is simple to incorporate source terms within the structure of multidimensional upwind schemes by decomposing them in the same manner as the flux terms [9]. For the approximate diagonalization approach this results in a slightly different residual to (42), namely

$$\mathbf{R}_T \;=\; \sum_{k=1}^{N_{eq}} (\lambda^k \cdot \nabla w^k + q^k - s_W^k)\, \mathbf{r}_c^k\;, \tag{55}$$

where s_W^k are the components of $\mathbf{S}_W = \frac{\partial \mathbf{W}}{\partial \mathbf{U}}\mathbf{S}$ (or, when a preconditioner is included, $\mathbf{S}_W = \frac{\partial \mathbf{W}}{\partial \mathbf{Q}}\mathbf{P}\frac{\partial \mathbf{Q}}{\partial \mathbf{U}}\mathbf{S}$). Each component of (55) is distributed using the coefficients calculated for the homogeneous equations. When simple wave models are used the correct treatment is not so obvious, since the components of the decomposition are not independent, and this represents a subject for further research.

7 Numerical results

The first test case presented here is that of flow through a symmetric constricted open channel of length 4, whose breadth is given by

$$B(x) \;=\; \begin{cases} 1.0 - (1.0 - B_{\min})\cos^2(\pi(x-2.0)) & \text{for} \quad |x-2.0| \;\leq\; 0.5 \\ 1.0 & \text{otherwise}\,, \end{cases} \tag{56}$$

where $B_{\min} = 0.92$ is the minimum channel breadth and x is the distance into the channel (so the throat is positioned at the midpoint of the constriction, $x = 2.0$). The 2114 node, 4054 cell grid on which the numerical results have been obtained is shown in Fig. 1 along with three steady state solutions distinguished by their freestream Froude numbers: (i) $F_\infty = 0.5$, completely subcritical and hence symmetric about the throat of the channel, (ii) $F_\infty = 0.71$, transcritical with a stationary hydraulic jump in the constriction downstream of the throat, and (iii) $F_\infty = 2.0$, completely supercritical, with a criss-cross pattern of undular jumps downstream of the throat. Simple characteristic boundary conditions are applied in each case. The solutions have been obtained using the hyperbolic/elliptic decomposition described in Section 5, applying the PSI scheme to each of the decoupled scalar components and a system Lax-Wendroff scheme to the subcritical elliptic subsystem. The results illustrate that the scheme can accurately model each of these different types of steady state flow.

It is interesting here to also present one preliminary result to illustrate the improvement which incorporating source terms within the decomposition makes over standard pointwise approximations. A straight open channel with a sinusoidal bump on its bed is used as the test case with a subcritical steady state flow over it, for which the discharge should be constant throughout the domain. Fig. 2 shows that the decomposed source term maintains this constant quantity at the level predicted by the exact solution whereas the pointwise evaluation shows significant errors.

Results from experimental test cases are presented, proposed by Prof. Zech (Civil Engineering Dept., UCL Belgium) from the Working Group on Dam Break Flow Modelling in which the authors are involved. Experimental and numerical results will be compared in these two time-dependent test cases. The treatment of the solution at the boundaries has been kept as close as possible to the theory of the characteristics in 2D. In all cases, the number of physical conditions to be imposed has been determined by this theory.

4.1 Test1: L-shaped channel

The flow domain, depicted in Fig. 3, consists of a square reservoir that initially contains a wall to separate it from the L-shaped channel. The initial conditions are zero flow with 0.2m depth to the left and 0.01m depth to the right of the wall. All boundaries are solid non-slip walls except the outlet which is considered free. The Manning coefficient is 0.0095 and the bed slope is zero. The number of elements used in the mesh is 2954. Comparisons of the time evolution of the depth of water predicted by experiment and numerics once the wall is removed

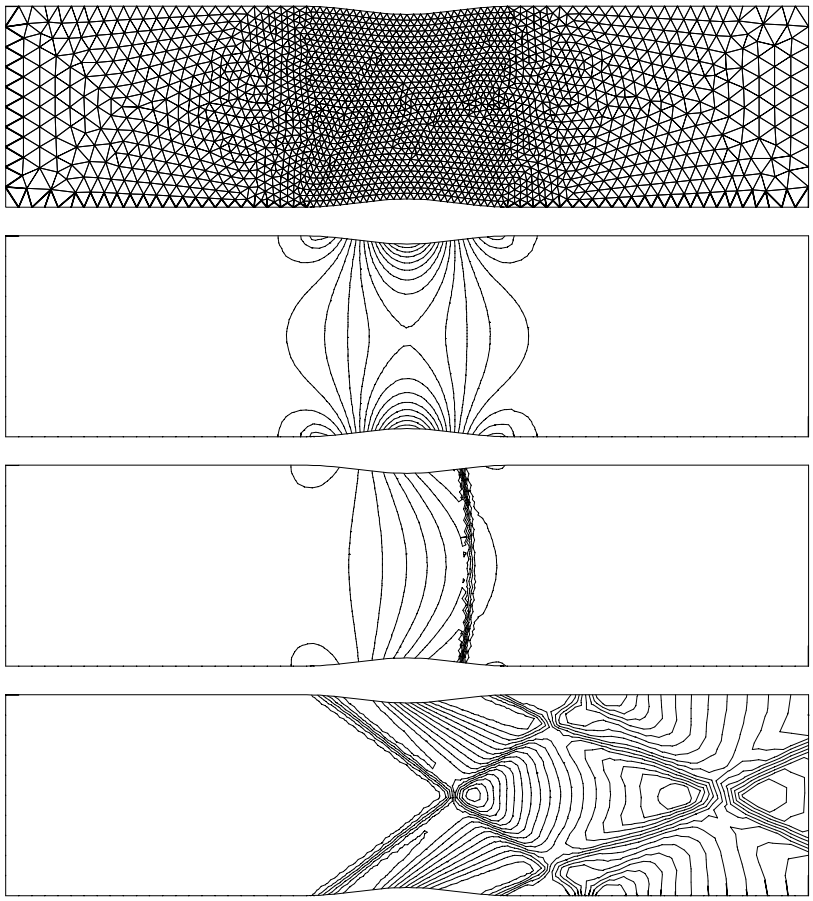

Figure 1: The grid and contours of depth for solutions of the subcritical (top), transcritical (middle) and supercritical (bottom) symmetric constricted open channel test cases.

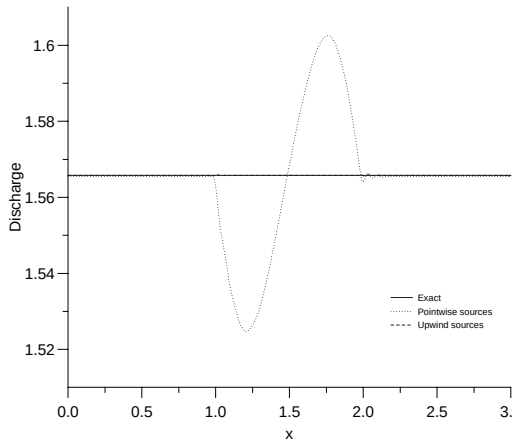

Figure 2: Solutions for the symmetric open channel with varying bed.

(using the ..... scheme) are made at the points P1, P2, P3, P4, P5 and P6, and are shown in Fig. 7. They indicate that the multidimensional upwind schemes do provide an accurate numerical model of the flow.

a)

Figure 3: Geometry for the L-shaped channel test.

4.3 Test2: Comparison with upwind finite volume scheme results
Results will now be presented which are obtained with first order upwind finite volume and multidimensional upwind (WHICH ONE??) approximations on the same unstructured Delaunay triangular mesh for a second experimental test case, also proposed by Prof. Zech.

The test to be studied combines a square shaped upstream reservoir and a channel with a 45° bend (see Fig. 5). The channel is made of 4.25m and 4.15m long and 0.495m wide rectilinear reaches connected at a 45° angle by an element.

a)

Figure 4: Time evolution of the depth of water at points P1 to P6 for Test1.

There is no slope in the channel. A gate (which is opened at $t = 0$) connects the channel to a 2.44m $\times$ 2.39m reservoir. The initial conditions are water at rest with the free surface 25cm above the bed level in the upstream reservoir and 1cm water depth in the channel. All boundaries are solid walls except the outlet which is considered free. The Manning coefficient is $n_b = 0.0095$ for the bed and $n_w = 0.0195$ for the walls. The number of elements used in the mesh is 15397.

The flow will be essentially two-dimensional in the reservoir and at the angle between the two straight reaches of the channel. Two features of the resulting dam break flow are of special interest: the damping effect of the corner, and the upstream moving hydraulic jump which is formed by reflection at the corner.

Nine gauging points were used in the laboratory to measure water level in time. Their locations are shown in Fig. 5. The measurements at these stations are

a)

Figure 5: Plane view of the Test2 channel with gauging points.

compared with the numerical results and displayed in Figs. 6 and 7. Fig. 8 shows snapshots of the free surface at time 18s.

In general, the figures indicate good performance of both numerical schemes. The arrival times of the main shock fronts is better captured by the standard upwind method. Some differences are noticeable in P2, P3 and P4 in terms of the reflected shock front celerity, which may be attributed to the treatment of the boundary conditions. However, the great improvement shown by the multidimensional upwinding is only really visible in the free surface plots, in which it is clear that it models the shock structure far better. This indicates that perhaps measurements along the walls of the channel should be taken into account to demonstrate which approximation is better. Up to now, only data in the central axis have been measured.

8 Conclusions

Two-dimensional wave decomposition and multidimensional upwinding seem a promising method of solution for the 2D shallow water equations. A number of schemes have been adapted to render the technique suited to hydraulic problems with shocks. As with the 1D TVD schemes, our experience with using the multidimensional upwind approach for the shallow water equations has closely followed that of the researchers solving the Euler equations (with both the advection schemes and the wave models), showing the same properties as for that system of equations.

The procedure is more complicated and costly than the most efficient present day generalizations of 1D upwind finite volume techniques. However, it is based on a triangular discretization and, by taking advantage of the triangles, the disadvantages can be overcome, making the schemes very competitive. The future for these schemes then looks much more promising, since they can clearly be applied to arbitrary geometries, a great advantage for hydraulic engineers working on practical problems, particularly as there is a wide variety of possibilities concerning grid movement and adaptation [7, 1].

(a) (b) (c) (d)

Figure 6: Water depth history at points a) P1, b) P2, c) P3 and d) P4 for Test2.

Future work is envisaged to find better ways to deal with the source terms present in the shallow water equations when applied to realistic problems, while there is still much work to be done in the development of more efficient and accurate schemes in unsteady cases, possibly following recent work on the scalar schemes[10, 13] but definitely requiring a more detailed study of possible wave models for time-dependent problems.

References

[1] M.J. Baines and M.E. Hubbard, Multidimensional upwinding with grid adaptation, in Numerical Methods for Wave Propagation, E.F.Toro and J.F.Clarke (Eds.), pp. 33–54, Kluwer Academic Publishers (1998).

[1] S.F. Davis, A rotationally biased upwind difference scheme for the Euler equations., J. Comput. Phys., 56 (1984).

(e) (f) (g) (h)

Figure 7: Water depth history at points e) P5, f) P6, g) P7 and h) P8 for Test2.

a)

Figure 8: Free surface at time t=18s for Test2 with upwind finite volume (left) and multidimensional upwind schemes (right).

[2] H. Deconinck, C. Hirsch, J. Peuteman, Characteristics decomposition methods for the multidimensional Euler equations, 10th Int. Conf. in Num. Met. in Fluid Dyn. 216-221 (1986).

[3] H. Deconinck, P.L. Roe and R. Struijs, A multi-dimensional generalization of Roe's flux difference splitter for the Euler equations, Computers and Fluids, 22:215–222 (1993).

[4] H. Deconinck, R. Struijs, G. Bourgois, H. Paillere, P.L. Roe, Multidimensional upwind methods for unstructured grids, Unstructured grid methods for advection dominated flows, AGARD787 (1992).

[5] H. Deconinck, R. Struijs, G. Bourgois and P.L. Roe, High resolution shock capturing cell vertex advection schemes for unstructured grids, in VKI LS 1994-05, Computational Fluid Dynamics (1994).

[6] H. Deconinck, Analysis of wave propagation properties for the Euler equations in two-space dimensions, in VKI LS 1994-05, Computational Fluid Dynamics (1994).

[7] H. Deconinck, B. Koren (editors), Euler and Navier-Stokes solvers using multidimensional upwind schemes and multigrid acceleration, Notes on Numerical Fluid Mechanics, volume 57, Vieweg (1997).

[8] M.E. Hubbard, Aspects of multidimensional upwinding: time-dependent nonlinear systems, source terms, spherical geometries, and three-dimensional grid adaptation, Report NA-4/99, Dept. of Math., Univ. of Reading, UK (1999).

[9] M.E. Hubbard and M.J. Baines, Conservative multidimensional upwinding for the steady two dimensional shallow water equations, J. Comput. Phys., 138:419–448 (1997).

[10] M.E. Hubbard and P.L. Roe, Compact high-resolution algorithms for time-dependent advection on unstructured grids, to appear, Int. J. for Num. Methods in Fluids (1999).

[11] R.J. LeVeque, Numerical methods for conservation laws, Birkhauser, Basel, 2nd edition (1992).

[12] D. Levy, K.G. Powell, B. Van Leer, Implementation of a grid-independent upwind scheme for the Euler equations, 91-0635, AIAA (1991).

[13] J. Marz, Improving time accuracy for residual distribution schemes, VKI PR 1996-17, von Karman Institute for Fluid Dynamics (1996).

[14] L.M. Mesaros and P.L. Roe, Multidimensional fluctuation splitting schemes based on decomposition methods, AIAA Paper 95-1699 (1995).

[15] H. Paillere, E. van der Weide and H. Deconinck, Multidimensional upwind methods for inviscid and viscous compressible flows, in VKI LS 1995-02, Computational Fluid Dynamics (1995).

[16] I.M. Parpia and D.J. Michalek, Grid-independent upwind scheme for multidimensional flow, AIAA J., 31(4): 646-651 (1993).

[17] P.L. Roe, Discrete models for the numerical analysis of time-dependent multidimensional gas dynamics, J. Comput. Phys., 63, pp 458-476 (1986).

[18] P.L. Roe, A basis for upwind differencing of the two-dimensional unsteady Euler equations, Num. Met. for Fluid Dyn. II, pp 55-80 (1986).

[19] M.A. Rudgyard, Multidimensional wave decompositions for the Euler equations, VKI Lecture notes (1993).

[20] C.L. Rumsey, B. Van Leer, P.L. Roe, A grid-independent approximate Riemann solver with applications to the Euler and Navier-Stokes equations, 91-1530, AIAA (1991).

[21] D. Sidilkover and P.L. Roe, Unification of some advection schemes in two dimensions, ICASE Report 95-10 (1995).

[22] Y. Tamura and K. Fujii, A multidimensional upwind scheme for the Euler equations on unstructured grids, 4th ISCFD Conference (1991).

[23] H.C. Yee, Report NASA TM-101088 (1989).